How to cite: *Angew. Chem. Int. Ed.* **2022,** *61,* e202213032
International Edition: doi.org/10.1002/anie.202213032
German Edition: doi.org/10.1002/ange.202213032

VIP **Iron–Sulfur Clusters** **Very Important Paper**

The Elusive Mononitrosylated [Fe_4S_4] Cluster in Three Redox States

*Youngsuk Kim, Arun Sridharan, and Daniel L. M. Suess**

Abstract: Iron-sulfur clusters are well-established targets in biological nitric oxide (NO) chemistry, but the key intermediate in these processes—a mononitrosylated [Fe_4S_4] cluster—has not been fully characterized in a protein or a synthetic model thereof. Here, we report the synthesis of a three-member redox series of isostructural mononitrosylated [Fe_4S_4] clusters. Mononitrosylation was achieved by binding NO to a 3:1 site-differentiated [Fe_4S_4]$^+$ cluster; subsequent oxidation and reduction afforded the other members of the series. All three clusters feature a local high-spin Fe^{3+} center antiferromagnetically coupled to ^{3}[NO]$^-$. The observation of an anionic NO ligand suggests that NO binding is accompanied by formal electron transfer from the cluster to NO. Preliminary reactivity studies with the monocationic cluster demonstrate that exposure to excess NO degrades the cluster, supporting the intermediacy of mononitrosylated intermediates in NO sensing/signaling.

Introduction

Nitric oxide (NO) is a biologically important radical that serves as a signaling molecule and as a cytotoxic armamentarium against intracellular parasites.[1–6] In response to the latter processes, many bacteria have evolved NO sensing abilities. For example, *Streptomyces coelicolor* senses NO using the [Fe_4S_4] protein NsrR.[7–9] Other NO-responsive [Fe_4S_4] proteins include WhiB1,[10] SufR[11] (both from *Mycobacterium tuberculosis*), WhiD[12] (*Streptomyces coelicolor*), and FNR (*Escherichia coli*).[13]

Because of the biomedical importance of NO sensing and signaling, there has been considerable interest in the in vitro reactivity between NO and Fe–S proteins.[14–17] Reactions of [Fe_4S_4] proteins with NO typically produce one or more polynitrosylated products with proposed structures including Roussin's black anion (RBA, and/or its analogues with bridging thiolates), Roussin's red esters (RREs), and dinitrosyl iron complexes (DNICs) (Figure 1);[18–22] the mechanisms by which these products form are highly complex and the molecular-level basis for specific reaction outcomes remains under investigation.[23–27] Stopped-flow kinetics experiments suggest stepwise nitrosylation,[23–26] and a likely candidate for the first nitrosylation intermediate—one that could be common to all observed reaction products—is a mononitrosylated [Fe_4S_4] cluster (Figure 1). Although this species has not been generated cleanly or fully characterized, and thus little is known about its geometric and electronic structure, it has been detected using mass spectrometry in reactions of NsrR and WhiD with NO.[27]

Reactivity studies of synthetic Fe–S clusters with NO have provided important insights into the mechanism of NO-mediated Fe–S cluster degradation.[28,29] Like their biological counterparts, synthetic [Fe_4S_4] clusters typically react with NO to produce polynitrosylated species such as [$Fe_4S_4(NO)_4$]$^-$, RBA, RREs, and DNICs.[30–35] In these studies, efforts to obtain a mononitrosylated cluster by limiting NO stoichiometry or employing 3:1 site-differentiating ligands resulted in mixtures of polynitrosylated compounds and unreacted starting material.[30,31] As such, synthetic routes to well-defined, mononitrosylated [Fe_4S_4] clusters have yet to be reported. We herein show that, by employing synthetic [Fe_4S_4] clusters supported by sterically protective supporting ligands, the challenges associated with preparing a mononitrosylated [Fe_4S_4] cluster can be overcome. As described below, this enables the preparation and characterization of mononitrosylated [Fe_4S_4] clusters in three charge states, as well as an initial evaluation of their reactivity with additional NO.

Results and Discussion

Our laboratory has previously reported that chloride abstraction from $(IMes)_3Fe_4S_4Cl$ (**1-Cl**; IMes = 1,3-dimesitylimidazol-2-ylidene) in Et_2O using Na[BAr^F_4] ([BAr^F_4]$^-$ = tetrakis[3,5-bis(trifluoromethyl)phenyl]borate) produces [$(IMes)_3Fe_4S_4(Et_2O)$][BAr^F_4] ([**1-OEt$_2$**]$^+$); the stability afforded by the bulky *N*-heterocyclic carbene ligands maintains the cluster's 3:1 site-differentiation[36–42] (the same differentiation pattern for the [Fe_4S_4] cluster of NsrR; Figure 1),[8] and the labile Et_2O ligand can be substituted by other donors.[36,40,42] Here, we report that addition of stoichiometric $NO_{(g)}$ to [**1-OEt$_2$**]$^+$ (generated in situ) furnishes the mononitrosylated cluster [$(IMes)_3Fe_4S_4(NO)$][BAr^F_4] ([**1-NO**]$^+$) whose structure was confirmed by single-

[*] Prof. Dr. Y. Kim, Dr. A. Sridharan, Prof. Dr. D. L. M. Suess
Department of Chemistry, Massachusetts Institute of Technology, 77 Massachusetts Ave, Cambridge, MA 02139 (USA)
E-mail: suess@mit.edu
Prof. Dr. Y. Kim
Department of Chemistry, Pusan National University
Busan 46241 (Republic of Korea)

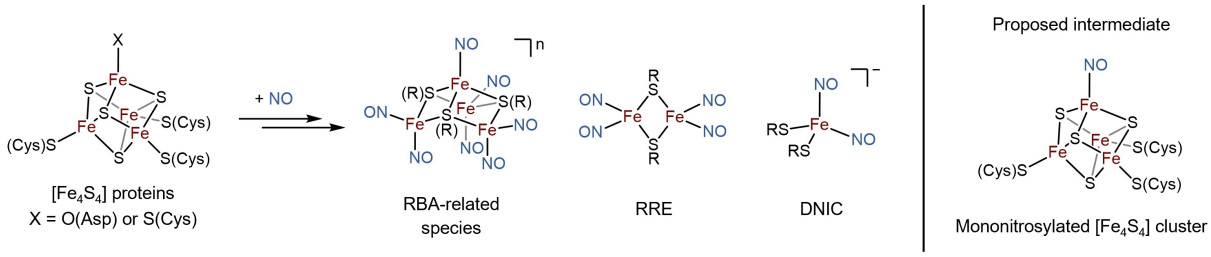

Figure 1. Reactivity of $[Fe_4S_4]$ proteins towards NO.

crystal X-ray diffraction (XRD; Figure 2). The Fe–NO unit of $[\mathbf{1\text{-}NO}]^+$ is essentially linear (∠Fe–N–O 178.3(3)°) with Fe–N and N–O bond lengths of 1.684(3) and 1.180(5) Å, respectively. As is common for cuboidal Fe–S clusters,[43,44] the $[Fe_4S_4]$ core is distorted from ideal T_d symmetry, with Fe–S bond lengths ranging from 2.253(1) Å to 2.298(1) Å (Table S1). The average Fe–S bond length (2.272(3) Å) falls within a range typical for $[Fe_4S_4]^{2+}$ clusters supported by three IMes ligands (for example, $[(IMes)_3Fe_4S_4(CH_2Ph)]^+$ has an average Fe–S bond length of 2.271(2) Å; see Table S7).[37] The three IMes ligands wrap around the cluster in a propeller-like fashion to give a pseudo-C_3 solid-state structure (Figure 2B). As with other $[(IMes)_3Fe_4S_4]$ clusters,[36,37,39–42] Fe–C bond rotation leads to C_{3v} symmetry in solution on the NMR timescale. The cluster's IR spectrum

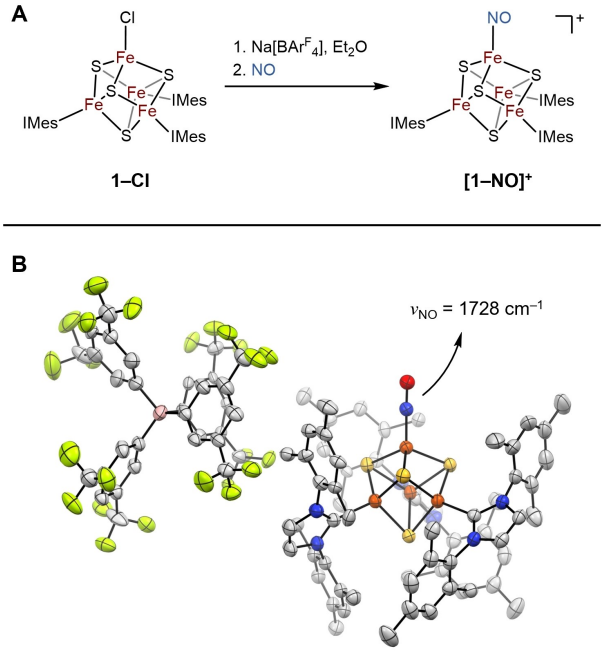

Figure 2. A) Synthesis of the mononitrosylated $[Fe_4S_4]$ cluster $[\mathbf{1\text{-}NO}]^+$. B) Solid-state structure of $[\mathbf{1\text{-}NO}]^+$ from single-crystal XRD analysis. The thermal ellipsoids are shown at the 30% probability level. Hydrogen atoms, solvent molecules, and disorders are omitted for clarity.

features a strong band corresponding to the N–O stretching mode at $\nu_{NO} = 1728\ cm^{-1}$ (Figure 2B and Figure 3C; see below). Variable-temperature SQUID magnetometry measurements revealed an $S = 1$ ground spin state (Figure S15); in contrast, most even-electron $[Fe_4S_4]$ clusters are $S = 0$,[45] and this unusual property of $[\mathbf{1\text{-}NO}]^+$ is discussed further below.

The cyclic voltammogram of $[\mathbf{1\text{-}NO}]^+$ shows two reversible waves at $E_{1/2} = -1.49$ V and -0.11 V (vs. Fc/Fc^+) that correspond to one-electron reduction and one-electron oxidation, respectively (Figure 3B). Accordingly, we undertook the synthesis of the reduced and oxidized congeners of $[\mathbf{1\text{-}NO}]^+$. Reaction between $[\mathbf{1\text{-}NO}]^+$ and $CoCp^*_2$ in benzene resulted in the formation of $[(IMes)_3Fe_4S_4(NO)]$ (**1-NO**) as characterized by the lower ν_{NO} at 1657 cm^{-1} (Figure 3A,C). Single-crystal XRD analysis (Figure 3E) confirmed the structure as a neutral, mononitrosylated $[Fe_4S_4]$ cluster, and revealed linear NO coordination (∠Fe–N–O = 170.6(2)°). Compared with $[\mathbf{1\text{-}NO}]^+$, **1-NO** has a longer average Fe–S bond length (2.282(2) Å vs. 2.272(3) Å), which is consistent with reduction of the $[Fe_4S_4]$ core. The X-band EPR spectrum of **1-NO** at 15 K features a rhombic signal with $g = [2.094, 2.058, 2.014]$ ($g_{avg} = 2.055$), indicative of an $S = {}^1/_2$ ground spin state (Figure S12A).

One-electron oxidation of $[\mathbf{1\text{-}NO}]^+$ using $[Cp_2Fe][BAr^F_4]$ resulted in the formation of the isostructural, dicationic cluster $[(IMes)_3Fe_4S_4(NO)][BAr^F_4]_2$ ($[\mathbf{1\text{-}NO}]^{2+}$) (Figure 3A). The value of ν_{NO} (1802 cm^{-1}) is higher than that of $[\mathbf{1\text{-}NO}]^+$ (1728 cm^{-1}; Figure 3C). Similarly to **1-NO** and $[\mathbf{1\text{-}NO}]^+$, linear NO coordination (∠Fe–N–O = 177.5(2)°) was observed from single-crystal XRD analysis (Figure 3F). Oxidation of the $[Fe_4S_4]$ core was evidenced by a significantly shorter average Fe–S bond length (2.222(2) Å) compared to $[\mathbf{1\text{-}NO}]^+$ (2.272(3) Å). The X-band EPR spectrum of $[\mathbf{1\text{-}NO}]^{2+}$ at 5 K features a broad, pseudo-axial signal whose crossing point ($d\chi''/dB = 0$) occurs at $g = 1.73$ (Figure S12B). The EPR spectra of $[\mathbf{1\text{-}NO}]$ and $[\mathbf{1\text{-}NO}]^{2+}$ thus reveal an $S = {}^1/_2$ ground spin state for both clusters with g_{avg} values above and below g_e, respectively. Although the direction that g_{avg} deviates from g_e is often a signature for the $[Fe_4S_4]$ cluster core charge state (with $[Fe_4S_4]^+$ and $[Fe_4S_4]^{3+}$ clusters typically exhibiting $g_{avg} < g_e$ and $g_{avg} > g_e$, respectively)[46] we note that such trends do not hold in all cases, particularly for clusters with π-acidic ligands,[36] and we therefore do not further interpret the g_{avg} values for $[\mathbf{1\text{-}NO}]$ and $[\mathbf{1\text{-}NO}]^{2+}$.

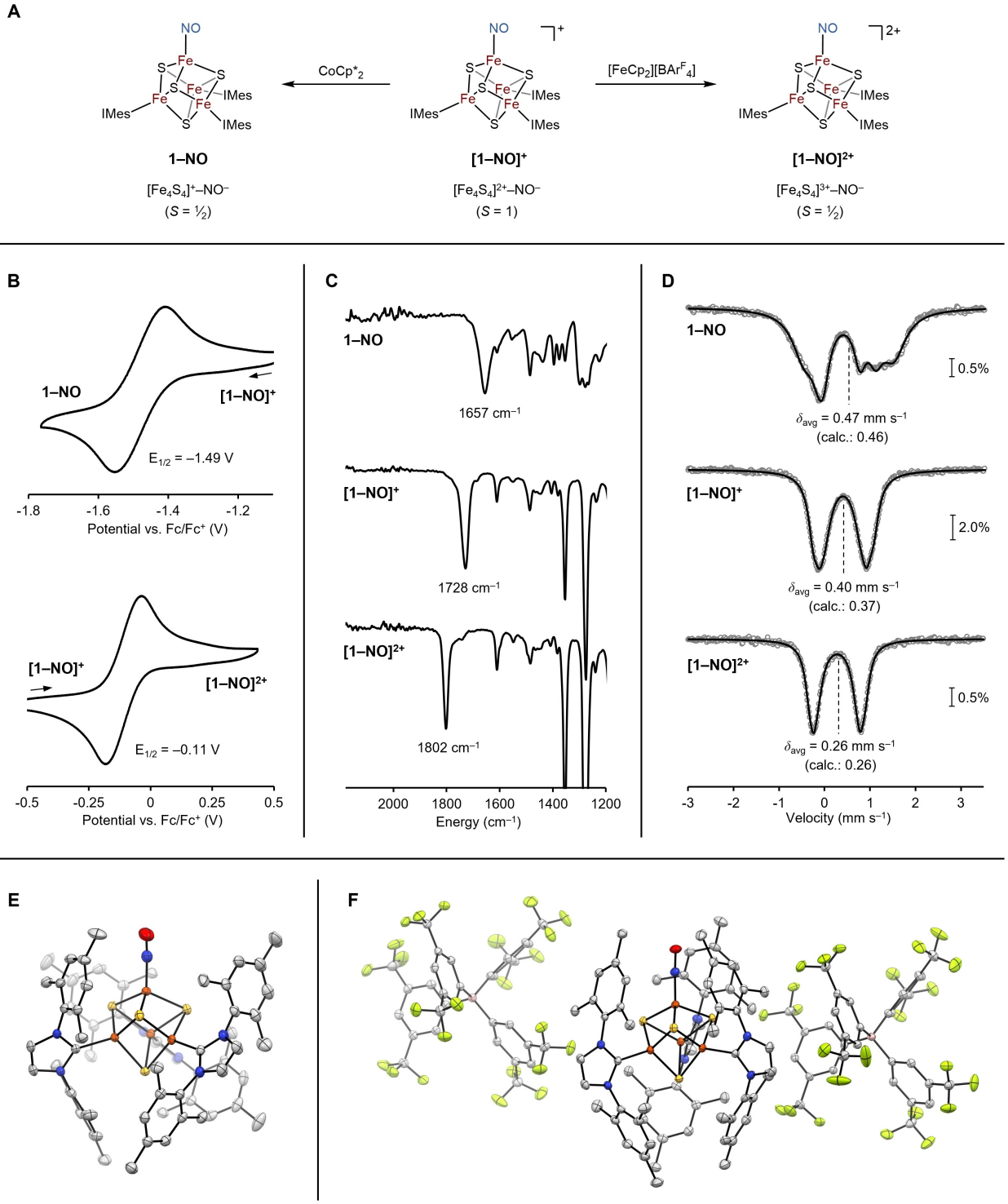

Figure 3. Synthesis and characterization of the three-member redox series. A) Synthetic scheme. B) Cyclic voltammograms of [**1-NO**]$^{+}$ (2 mM) in *o*-difluorobenzene towards negative (top) and positive (bottom) potentials. Scan rate, 0.1 V s^{-1}; electrolyte, 0.1 M [Bu_4N][PF_6]. C) FT-IR spectra of **1-NO** (top), [**1-NO**]$^{+}$ (middle), and [**1-NO**]$^{2+}$ (bottom). N–O stretching frequencies are labeled. D) Zero-field ^{57}Fe Mössbauer spectra (80 K) of **1-NO** (top), [**1-NO**]$^{+}$ (middle), and [**1-NO**]$^{2+}$ (bottom) with experimental data (circles), total simulation (solid line; see Supporting Information for details), and spectral centroid (giving δ_{avg}, as indicated). DFT-calculated δ_{avg} values are shown in parenthesis (see Supporting Information for details). E) Solid-state structures of **1-NO** and F) [**1-NO**]$^{2+}$ from single-crystal X-ray crystallography. The thermal ellipsoids are shown at the 50% probability level. Hydrogen atoms, solvent molecules, and disorders are omitted for clarity.

Having prepared and characterized the three-member redox series of mononitrosylated $[Fe_4S_4]$ clusters, we next undertook a comparative analysis of the clusters' properties to gain insights into their electronic structures. Although the bonding in these species is exceptionally complicated owing to the possibility for redox-noninnocence of the nitrosyl ligand (i.e., NO^-, $NO^\bullet$, or NO^+) and the multiconfigurational nature of both Fe–S clusters and Fe–NO complexes, the spectroscopic data, particularly analysis of ν_{NO}, allows us to comment on the major resonance contributors to the electronic structures of the [**1-NO**]^n series.

The difference in NO stretching frequency ($\Delta\nu_{NO}$) across the redox series is approximately 70 cm^{-1} per one-electron redox event (Figure 3C), indicative of modest changes in N–O π* orbital population. Indeed, the magnitude of $\Delta\nu_{NO}$ is much lower than that observed for redox series of iron nitrosyls in which the redox events are thought to be localized at NO ($\Delta\nu_{NO}$ = 200–300 cm^{-1}; see Table S8).[47–50] Redox series of mononuclear iron nitrosyl complexes having smaller $\Delta\nu_{NO}$ values of *ca.* 90–150 cm^{-1} have been reported, and in these cases the redox events are thought to occur primarily at Fe orbitals not involved in Fe–NO π-bonding.[51–56] The even smaller value of $\Delta\nu_{NO}$ for the [**1-NO**]^n series indicates that the electron transfer events do not occur primarily on the nitrosyl group, and instead points to substantial changes in charge at the $[Fe_4S_4]$ cluster core. This conclusion is supported by the decrease in average Mössbauer isomer shift (δ_{avg}) across the [**1-NO**]^n series, from 0.47 $mm\,s^{-1}$ for **1-NO** to 0.40 and 0.26 $mm\,s^{-1}$ for [**1-NO**]$^+$ and [**1-NO**]$^{2+}$, respectively (Figure 3D). The decrease in δ_{avg} across the series is comparable to what has been reported for $[Fe_4S_4]$ clusters that undergo cluster-centered oxidation events (typically, a decrease in δ_{avg} of approximately 0.1 $mm\,s^{-1}$ per electron).[57] Note that other mononitrosylated $[Fe_4O]$ or $[FeV_5]$ clusters have been characterized in multiple charge states, with $\Delta\nu_{NO}$ values of *ca.* 30–40 cm^{-1};[58,59] in these examples, the lower $\Delta\nu_{NO}$ values are consistent with weaker coupling between the redox-active metals and the Fe–NO fragment than in the [**1-NO**]^n series.

The N–O stretching frequency for the middle member of this series, [**1-NO**]$^+$ (ν_{NO} = 1728 cm^{-1}) is strikingly similar to that reported for its structurally closest mononuclear analogues: the four-coordinate, thiolate-supported $[(SR)_3Fe(NO)]^-$ complexes (ν_{NO} = 1731 and 1704 cm^{-1} for R = Ph and ^{t}Bu, respectively),[60,61] which likewise feature nearly linear Fe–N–O angles. The mononuclear complexes adopt a dominant Fe^{3+}-$[NO]^-$ configuration, where the $[^3NO]^-$ ligand is antiferromagnetically coupled to a high-spin Fe^{3+} ion.[60] Based on the structural and spectroscopic similarities between $[(SR)_3Fe(NO)]^-$ complexes and the NO-bound Fe in [**1-NO**]$^+$, as well as the modest change in ν_{NO} across the [**1-NO**]^n series, we conclude that the NO-bound Fe centers in the [**1-NO**]^n series are best described as high-spin Fe^{3+} ions antiferromagnetically coupled to $[^3NO]^-$ ligands. Previous computational studies[62,63] have also favored an antiferromagnetically coupled, high-spin Fe^{3+}-$[^3NO]^-$ configuration for the iron-nitrosyl fragments in polynitrosylated Fe–S clusters, and this assignment is likewise supported by our DFT calculations on the mononitrosylated clusters reported herein (see below).

Broken symmetry density functional theory (BS-DFT) calculations (TPSSh/DKH-def2-TZVP) were performed on models derived from the crystallographic coordinates (Mes groups were truncated to H, and all H atom positions were optimized; see Supporting Information for details). We first note that the calculated Mössbauer parameters align with the experimental δ_{avg} values for all members of the series (Figure 3D and Table S6). Localized molecular orbital (LMO) analysis of the lowest-energy BS-DFT determinants of **1-NO**, [**1-NO**]$^+$, and [**1-NO**]$^{2+}$ reveals a $[^3NO]^-$ ligand bound to $[Fe_4S_4]^{1+}$, $[Fe_4S_4]^{2+}$, and $[Fe_4S_4]^{3+}$ cluster cores, respectively (Figure 4 and Figure S14).[64–66] Specifically, **1-NO** is comprised of a ferrous pair ($2\times Fe^{2+}$) and a mixed-valent pair (Fe^{2+}/Fe^{3+}) leading to the $S = {}^1/_2$ ground state of typical $[Fe_4S_4]^{1+}$ clusters, and the cluster is further antiferromagnetically coupled to the $[^3NO]^-$ ligand to give overall an $S = {}^1/_2$ ground state (Figure 4A). The mixed-valent pair has an asymmetric coordination sphere (one bound to $[NO]^-$ (Fe1) and the other to IMes (Fe2)), resulting in asymmetric electron delocalization and substantial Fe^{3+} character at the Fe1 center.[39,67] Löwdin population analysis of this LMO (represented as the blue electron in Figure 4A) shows 18 % and 74 % contributions from Fe1 and Fe2, respectively. The near-localization of Fe^{3+} character at Fe1 is also supported by our preferred (albeit tentative) simulation of the Mössbauer spectra (Figure S6 and Table S6), where Fe1 is distinguished by the lowest isomer shift (0.37 $mm\,s^{-1}$, versus 0.48–0.52 $mm\,s^{-1}$ for the other iron sites).

LMO analysis of [**1-NO**]$^+$ reveals that the ferric character of Fe1 is maintained upon oxidation of **1-NO** (Table S5; see Supporting Information for detailed computation results). For [**1-NO**]$^+$, two mixed-valent pairs—typical for an $[Fe_4S_4]^{2+}$ cluster[65]—are now found, with the Fe1–Fe2 pair again exhibiting polarization of the itinerate electron, resulting in Fe^{3+} character for Fe1 (Figure 4B). As expected, the other mixed-valent pair (Fe3/Fe4, each with an identical primary coordination sphere) exhibits symmetric valence delocalization (electron indicated by the purple arrow in Figure 4B). The unusual, experimentally observed $S = 1$ ground state is rationalized in the computations by standard, pairwise antiferromagnetic coupling within the $[Fe_4S_4]^{2+}$ core, and further antiferromagnetic coupling to the $[^3NO]^-$ ligand (Figure 4B).

We were not able to clearly identify a single low-energy BS configuration for [**1-NO**]$^{2+}$, and we are therefore reluctant to discuss the most plausible resonance forms of [**1-NO**]$^{2+}$ (see Figure S14 for details). Nevertheless, the two nearly isoenergetic, lowest-energy configurations exhibit an $[Fe_4S_4]^{3+}$-$[^3NO]^-$ configuration with substantial Fe^{3+} character for the nitrosylated Fe, in line with our spectroscopic analysis.

Lastly, we explored the reactivity of [**1-NO**]$^+$ toward additional NO equivalents. Previous work[30] has shown that $[Et_4N]_2[Fe_4S_4(SPh)_4]$ reacts with excess NO and $[Et_4N][SPh]$ to yield the DNIC $[Et_4N][Fe(NO)_2(SPh_2)]$ and that a similar reaction takes place with trityl thionitrite (Ph_3CSNO) as an NO donor in the presence of excess thiophenol and $[Et_4N]$-

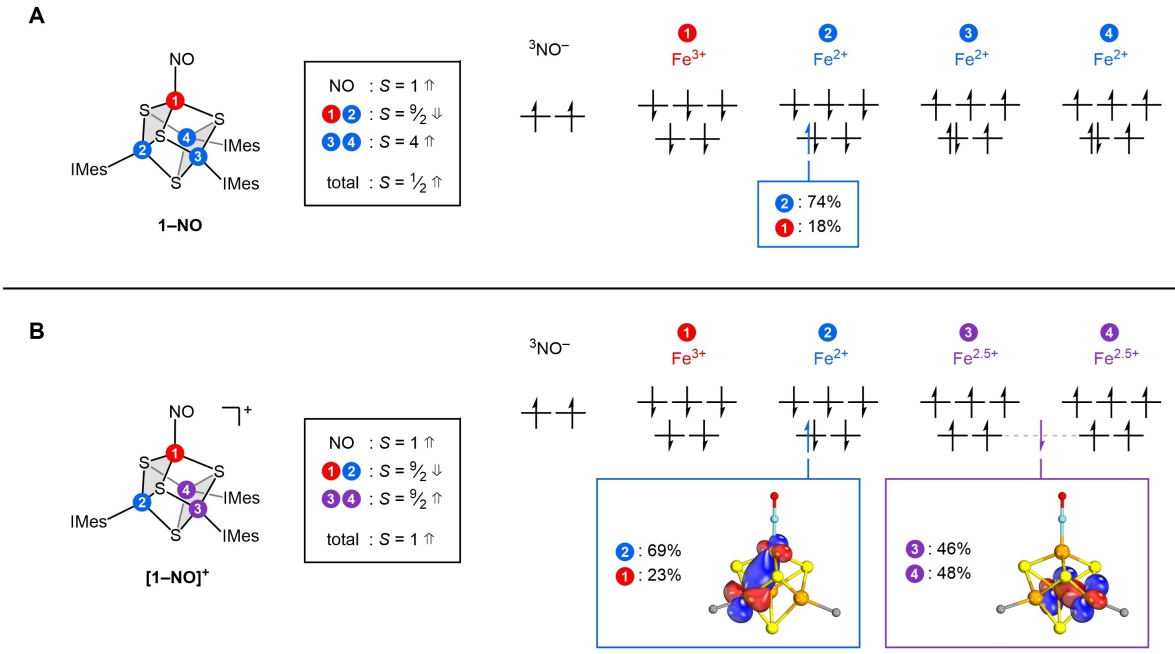

Figure 4. Qualitative frontier orbital diagrams for A) **1-NO** and B) [**1-NO**]$^+$ from BS-DFT calculations. Rhombs containing spin-aligned Fe atoms are highlighted in gray. Orbital isosurface plots (encompassing 85 % of the orbital's total electron density) are drawn for the colored LMOs of [**1-NO**]$^+$. Relative contributions from associated Fe atoms (obtained from a Löwdin population analysis) are indicated for select LMOs.

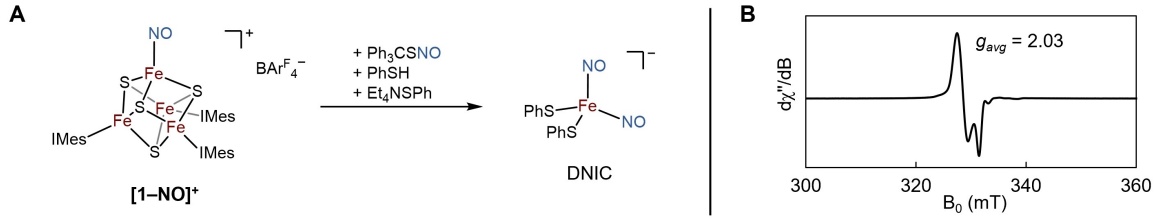

Figure 5. Reactivity of [**1-NO**]$^+$ with additional NO. A) Reaction resulting in the formation of a DNIC. B) EPR spectrum of the reaction mixture with a characteristic DNIC signal.

[SPh].[34] The production of DNICs by these synthetic models therefore mimics aspects of the reactivity of biological [Fe_4S_4] clusters toward NO; however, the mechanisms of such reactions remain unclear. Given this precedent, we added excess Ph_3CSNO to [**1-NO**]$^+$ in the presence of excess thiophenol and [Et_4N][SPh] to see if a DNIC would be formed. Rapid consumption of [**1-NO**]$^+$ was observed, accompanying a color change from brown to dark red. EPR spectroscopic characterization of the reaction mixture revealed a distinct axial EPR signal at $g_{avg}=2.03$ (Figure 5 and Figure S11) that is a signature of a DNIC.[68] Additionally, the IR spectrum of the product features two strong absorptions at 1740 and 1691 cm^{-1} (Figure S10), further confirming the generation of [Et_4N][$Fe(NO)_2(SPh_2)$].[35] Based on these findings, we conclude that the mononitrosylated cluster [**1-NO**]$^+$ is a competent intermediate en route to DNIC formation.

Conclusion

In summary, a mononitrosylated [Fe_4S_4] cluster was synthesized by the addition of NO to a 3:1 site-differentiated [Fe_4S_4] cluster, and a three-member redox series was generated by subsequent one-electron reduction and oxidation. While these clusters are highly multiconfigurational, experimental and computational studies suggest that the major resonance contributors to the electronic structures of the [**1-NO**]^n ($n=0$, $1+$, $2+$) series are [Fe_4S_4]$^+$-[NO]$^-$, [Fe_4S_4]$^{2+}$-[NO]$^-$, and [Fe_4S_4]$^{3+}$-[NO]$^-$, respectively; the iron nitrosyl fragment is best described as an {Fe–NO}^{7} species ([^{3}NO]$^-$ antiferromagnetically coupled to high-spin Fe^{3+}) regardless of the cluster charge state. The finding that each member of the redox series features a reduced NO ligand suggests that biological [Fe_4S_4] clusters, regardless of their core charge state, likely bind NO with formal one-electron

oxidation of the cluster. This behavior resembles that observed in O_2 chemistry, where O_2 coordinates to metal centers with formal electron transfer.[69,70] Finally, the finding that a DNIC is generated upon reaction of $[\mathbf{1\text{-}NO}]^+$ with excess NO lends additional credence to the intermediacy of mononitrosylated $[Fe_4S_4]$ intermediates in biological NO sensing.

Acknowledgements

We thank P. Müller for assistance with XRD experiments and M. Dincă for providing $NO_{(g)}$. This work was supported by the National Institute of General Medical Sciences of the National Institutes of Health under award number R01GM136882.

Conflict of Interest

The authors declare no conflict of interest.

Data Availability Statement

The data that support the findings of this study are available from the corresponding author upon reasonable request.

Keywords: Bioinorganic Chemistry · Cluster Compounds · Iron-Sulfur Clusters · Nitric Oxide · Nitrosyl Complexes

[1] A. J. Gow, H. Ischiropoulos, *J. Cell. Physiol.* **2001**, *187*, 277–282.
[2] E. Culotta, D. Koshland, *Science* **1992**, *258*, 1862–1865.
[3] V. Calabrese, C. Mancuso, M. Calvani, E. Rizzarelli, D. A. Butterfield, A. M. Giuffrida Stella, *Nat. Rev. Neurosci.* **2007**, *8*, 766–775.
[4] S. H. Snyder, *Science* **1992**, *257*, 494–6.
[5] D. Fukumura, S. Kashiwagi, R. K. Jain, *Nat. Rev. Cancer* **2006**, *6*, 521–534.
[6] J. MacMicking, Q. Xie, C. Nathan, *Annu. Rev. Immunol.* **1997**, *15*, 323–350.
[7] J. C. Crack, J. Munnoch, E. L. Dodd, F. Knowles, M. M. Al Bassam, S. Kamali, A. A. Holland, S. P. Cramer, C. J. Hamilton, M. K. Johnson, A. J. Thomson, M. I. Hutchings, N. E. Le Brun, *J. Biol. Chem.* **2015**, *290*, 12689–12704.
[8] A. Volbeda, E. L. Dodd, C. Darnault, J. C. Crack, O. Renoux, M. I. Hutchings, N. E. Le Brun, J. C. Fontecilla-Camps, *Nat. Commun.* **2017**, *8*, 15052.
[9] R. Rohac, J. C. Crack, E. de Rosny, O. Gigarel, N. E. Le Brun, J. C. Fontecilla-Camps, A. Volbeda, *Commun. Biol.* **2022**, *5*, 769.
[10] B. K. Kudhair, A. M. Hounslow, M. D. Rolfe, J. C. Crack, D. M. Hunt, R. S. Buxton, L. J. Smith, N. E. Le Brun, M. P. Williamson, J. Green, *Nat. Commun.* **2017**, *8*, 2280.
[11] K. Anand, A. Tripathi, K. Shukla, N. Malhotra, A. K. Jamithireddy, R. K. Jha, S. N. Chaudhury, R. S. Rajmani, A. Ramesh, V. Nagaraja, B. Gopal, G. Nagaraju, A. S. Narain Seshayee, A. Singh, *Redox. Biol.* **2021**, *46*, 102062.
[12] J. C. Crack, C. D. den Hengst, P. Jakimowicz, S. Subramanian, M. K. Johnson, M. J. Buttner, A. J. Thomson, N. E. Le Brun, *Biochemistry* **2009**, *48*, 12252–12264.
[13] H. Cruz-Ramos, J. Crack, G. Wu, M. N. Hughes, C. Scott, A. J. Thomson, J. Green, R. K. Poole, *EMBO J.* **2002**, *21*, 3235–3244.
[14] M. C. Kennedy, W. E. Antholine, H. Beinert, *J. Biol. Chem.* **1997**, *272*, 20340–20347.
[15] M. W. Foster, J. A. Cowan, *J. Am. Chem. Soc.* **1999**, *121*, 4093–4100.
[16] E. T. Yukl, M. A. Elbaz, M. M. Nakano, P. Moënne-Loccoz, *Biochemistry* **2008**, *47*, 13084–13092.
[17] E. L. Dodd, J. C. Crack, A. J. Thomson, N. E. Le Brun, in *Iron-Sulfur Clust. Chem. Biol.* (Ed.: T. Rouault), De Gruyter, Berlin, Boston, **2017**, pp. 387–437.
[18] C. E. Tinberg, Z. J. Tonzetich, H. Wang, L. H. Do, Y. Yoda, S. P. Cramer, S. J. Lippard, *J. Am. Chem. Soc.* **2010**, *132*, 18168–18176.
[19] Z. J. Tonzetich, H. Wang, D. Mitra, C. E. Tinberg, L. H. Do, F. E. Jenney, M. W. W. Adams, S. P. Cramer, S. J. Lippard, *J. Am. Chem. Soc.* **2010**, *132*, 6914–6916.
[20] P. N. Serrano, H. Wang, J. C. Crack, C. Prior, M. I. Hutchings, A. J. Thomson, S. Kamali, Y. Yoda, J. Zhao, M. Y. Hu, E. E. Alp, V. S. Oganesyan, N. E. Le Brun, S. P. Cramer, *Angew. Chem. Int. Ed.* **2016**, *55*, 14575–14579; *Angew. Chem.* **2016**, *128*, 14795–14799.
[21] L. A. Ekanger, P. H. Oyala, A. Moradian, M. J. Sweredoski, J. K. Barton, *J. Am. Chem. Soc.* **2018**, *140*, 11800–11810.
[22] J. C. Crack, C. J. Hamilton, N. E. Le Brun, *Chem. Commun.* **2018**, *54*, 5992–5995.
[23] J. C. Crack, L. J. Smith, M. R. Stapleton, J. Peck, N. J. Watmough, M. J. Buttner, R. S. Buxton, J. Green, V. S. Oganesyan, A. J. Thomson, N. E. Le Brun, *J. Am. Chem. Soc.* **2011**, *133*, 1112–1121.
[24] J. C. Crack, D. A. Svistunenko, J. Munnoch, A. J. Thomson, M. I. Hutchings, N. E. Le Brun, *J. Biol. Chem.* **2016**, *291*, 8663–8672.
[25] J. C. Crack, M. R. Stapleton, J. Green, A. J. Thomson, N. E. Le Brun, *J. Biol. Chem.* **2013**, *288*, 11492–11502.
[26] J. C. Crack, J. Green, A. J. Thomson, N. E. L. Brun, *Acc. Chem. Res.* **2014**, *47*, 3196–3205.
[27] J. C. Crack, N. E. Le Brun, *Chem. Eur. J.* **2019**, *25*, 3675–3684.
[28] J. Fitzpatrick, E. Kim, *Acc. Chem. Res.* **2015**, *48*, 2453–2461.
[29] Z. J. Tonzetich, L. E. McQuade, S. J. Lippard, *Inorg. Chem.* **2010**, *49*, 6338–6348.
[30] T. C. Harrop, Z. J. Tonzetich, E. Reisner, S. J. Lippard, *J. Am. Chem. Soc.* **2008**, *130*, 15602–15610.
[31] E. Victor, S. J. Lippard, *Inorg. Chem.* **2014**, *53*, 5311–5320.
[32] Z. J. Tonzetich, L. H. Do, S. J. Lippard, *J. Am. Chem. Soc.* **2009**, *131*, 7964–7965.
[33] C. T. Tran, E. Kim, *Inorg. Chem.* **2012**, *51*, 10086–10088.
[34] K. M. Oakley, Z. Zhao, R. L. Lehane, J. Ma, E. Kim, *Inorg. Chem.* **2021**, *60*, 15910–15917.
[35] F.-T. Tsai, S.-J. Chiou, M.-C. Tsai, M.-L. Tsai, H.-W. Huang, M.-H. Chiang, W.-F. Liaw, *Inorg. Chem.* **2005**, *44*, 5872–5881.
[36] A. C. Brown, D. L. M. Suess, *Inorg. Chem.* **2019**, *58*, 5273–5280.
[37] A. C. Brown, D. L. M. Suess, *J. Am. Chem. Soc.* **2020**, *142*, 14240–14248.
[38] A. McSkimming, D. L. M. Suess, *Nat. Chem.* **2021**, *13*, 666–670.
[39] A. Sridharan, A. C. Brown, D. L. M. Suess, *Angew. Chem. Int. Ed.* **2021**, *60*, 12802–12806; *Angew. Chem.* **2021**, *133*, 12912–12916.
[40] A. C. Brown, N. B. Thompson, D. L. M. Suess, *J. Am. Chem. Soc.* **2022**, *144*, 9066–9073.
[41] M. Ye, A. C. Brown, D. L. M. Suess, *J. Am. Chem. Soc.* **2022**, *144*, 13184–13195.

[42] A. C. Brown, D. L. M. Suess, *Inorg. Chem.* **2022**, https://doi.org/10.1021/acs.inorgchem.2c01353.
[43] L. L. Tan, R. H. Holm, S. C. Lee, *Polyhedron* **2013**, *58*, 206–217.
[44] L. Deng, A. Majumdar, W. Lo, R. H. Holm, *Inorg. Chem.* **2010**, *49*, 11118–11126.
[45] K. Rupnik, C. C. Lee, Y. Hu, M. W. Ribbe, B. J. Hales, *J. Am. Chem. Soc.* **2011**, *133*, 6871–6873.
[46] W. R. Hagen, *Adv. Inorg. Chem.* **1992**, *38*, 165–222.
[47] R. G. Serres, C. A. Grapperhaus, E. Bothe, E. Bill, T. Weyhermüller, F. Neese, K. Wieghardt, *J. Am. Chem. Soc.* **2004**, *126*, 5138–53.
[48] I. K. Choi, Y. Liu, D. Feng, K. J. Paeng, M. D. Ryan, *Inorg. Chem.* **1991**, *30*, 1832–1839.
[49] X. H. Mu, K. M. Kadish, *Inorg. Chem.* **1988**, *27*, 4720–4725.
[50] A. B. McQuarters, J. W. Kampf, E. E. Alp, M. Hu, J. Zhao, N. Lehnert, *Inorg. Chem.* **2017**, *56*, 10513–10528.
[51] M. J. Chalkley, J. C. Peters, *Angew. Chem. Int. Ed.* **2016**, *55*, 11995–11998; *Angew. Chem.* **2016**, *128*, 12174–12177.
[52] M. Keilwerth, J. Hohenberger, F. W. Heinemann, J. Sutter, A. Scheurer, H. Fang, E. Bill, F. Neese, S. Ye, K. Meyer, *J. Am. Chem. Soc.* **2019**, *141*, 17217–17235.
[53] A. L. Speelman, C. J. White, B. Zhang, E. E. Alp, J. Zhao, M. Hu, C. Krebs, J. Penner-Hahn, N. Lehnert, *J. Am. Chem. Soc.* **2018**, *140*, 11341–11359.
[54] A. L. Speelman, N. Lehnert, *Angew. Chem. Int. Ed.* **2013**, *52*, 12283–12287; *Angew. Chem.* **2013**, *125*, 12509–12513.
[55] A. L. Speelman, B. Zhang, C. Krebs, N. Lehnert, *Angew. Chem. Int. Ed.* **2016**, *55*, 6685–6688; *Angew. Chem.* **2016**, *128*, 6797–6800.
[56] C. Kupper, J. A. Rees, S. Dechert, S. DeBeer, F. Meyer, *J. Am. Chem. Soc.* **2016**, *138*, 7888–7898.
[57] P. Venkateswara Rao, R. H. Holm, *Chem. Rev.* **2004**, *104*, 527–59.
[58] G. de Ruiter, N. B. Thompson, D. Lionetti, T. Agapie, *J. Am. Chem. Soc.* **2015**, *137*, 14094–14106.
[59] F. Li, R. L. Meyer, S. H. Carpenter, L. E. VanGelder, A. W. Nichols, C. W. Machan, M. L. Neidig, E. M. Matson, *Chem. Sci.* **2018**, *9*, 6379–6389.
[60] T. C. Harrop, D. Song, S. J. Lippard, *J. Am. Chem. Soc.* **2006**, *128*, 3528–3529.
[61] T.-T. Lu, S.-J. Chiou, C.-Y. Chen, W.-F. Liaw, *Inorg. Chem.* **2006**, *45*, 8799–8806.
[62] K. H. Hopmann, A. Ghosh, L. Noodleman, *Inorg. Chem.* **2009**, *48*, 9155–9165.
[63] K. H. Hopmann, J. Conradie, A. Ghosh, *J. Phys. Chem. B* **2009**, *113*, 10540–10547.
[64] L. Noodleman, *Inorg. Chem.* **1991**, *30*, 246–256.
[65] L. Noodleman, C. Y. Peng, D. A. Case, J.-M. Mouesca, *Coord. Chem. Rev.* **1995**, *144*, 199–244.
[66] L. Noodleman, *Inorg. Chem.* **1988**, *27*, 3677–3679.
[67] M. Ye, N. B. Thompson, A. C. Brown, D. L. M. Suess, *J. Am. Chem. Soc.* **2019**, *141*, 13330–13335.
[68] A. R. Butler, I. L. Megson, *Chem. Rev.* **2002**, *102*, 1155–1166.
[69] P. L. Holland, *Dalton Trans.* **2010**, *39*, 5415.
[70] W. Nam, *Acc. Chem. Res.* **2015**, *48*, 2415–2423.
[71] Deposition numbers 2205001 (for **1-NO**), 2205003 (for **[1-NO]$^+$**), and 2205002 (for **[1-NO]$^{2+}$**) contain the supplementary crystallographic data for this paper. These data are provided free of charge by the joint Cambridge Crystallographic Data Centre and Fachinformationszentrum Karlsruhe Access Structures service.

Manuscript received: September 3, 2022
Accepted manuscript online: October 4, 2022
Version of record online: October 25, 2022